Geophysical Prospecting

EAGE EUROPEAN ASSOCIATION OF GEOSCIENTISTS & ENGINEERS

Geophysical Prospecting, 2020, **68**, 690–708 doi: 10.1111/1365-2478.12843

Generalized Tikhonov's algorithm for accurate calculation of one-dimensional transient responses directly in time domain

Vladimir Mogilatov[1,2] and Mark Goldman[3]*

[1]*Institute of Petroleum Geology and Geophysics, Novosibirsk 630090, Russia,* [2]*Novosibirsk State University, Novosibirsk 630090, Russia, and* [3]*University of Haifa, Haifa 3498838, Israel*

Received October 2018, revision accepted July 2019

ABSTRACT

In the last two decades, forward modelling for the time domain (transient) electromagnetic method has concentrated almost entirely on multi-dimensional models and algorithms. At the same time, the interpretation of real field data is still mainly one dimensional. This is caused by the lack of an efficient multi-dimensional acquisition procedure supported by sufficiently fast and reliable inversion software, on the one hand, and by the great efficiency of one-dimensional field set up and interpretation of the data on the other hand. The latter is particularly true for the short offset transient electromagnetic method, which is much less sensitive to multi-dimensional effects, compared to long offset methods. The most commonly used one-dimensional forward modelling algorithms are based on the spectral method, which requires calculating rapidly oscillating Fourier–Bessel (Hankel) integrals. Due to the very fast decay of short offset responses, the integrals become computationally unstable at late times of the transient process. Although this problem has been successfully solved for practically feasible measurement times of conventional short offset systems using transverse electric and mixed transverse electric and transverse magnetic fields, it turned out crucial for novel methods based on the use of unimodal transverse magnetic fields. These methods are much more sensitive to geoelectric parameters of the Earth in general and those of resistive targets, in particular, but they generate responses, which drop at late times significantly faster than those of conventional methods. Such behaviour of transverse magnetic fields represents severe computational problem for the spectral method, but is successfully solved by direct time domain algorithms. This article describes a generalization of the well-known Tikhonov's solution to a boundary value problem directly in time domain, which is applied to an arbitrary one-dimensional earth model excited by an arbitrary source. Contrary to existing spectral algorithms, the described method allows accurate calculations of both transverse electric and transverse magnetic transient responses at arbitrarily late times. On the other hand, it is more time efficient than finite-difference/finite element direct time domain algorithms and provides analytical late-stage asymptotic solutions.

Key words: Transient electromagnetic method, Modelling, 1D.

1 INTRODUCTION

There are two independent approaches for solving one-dimensional (1-D) forward problems in the transient electromagnetic (TEM) method. The first and the most commonly used one is based on either analytical or numerical solution to the boundary value problem for the Helmholtz equation in frequency domain (FD) followed by the inverse Fourier or Laplace transform of the obtained spectral function. This

*E-mail: mgol1302@gmail.com

method is customarily named the spectral method. The second method is also based on either an analytical or numerical solution to the boundary value problem for the heat (or diffusion) equation directly in time domain.

The spectral method gained a great popularity in modelling TEM fields mainly due to its generality as it can be applied to any model, for which an FD solution is calculated at sufficient number of frequencies. However, it also suffers from two significant drawbacks, which become crucial in certain cases. The first and main drawback stems from the necessity to carry out a numerical Fourier/Laplace transform of an FD kernel function, which inevitably becomes unstable at sufficiently late times. Another drawback, only relevant to 1-D problems, is inability of the method to provide analytical late time asymptotic solutions for arbitrary arrays and resistivities of the basement. These are very useful for understanding physical processes and evaluating an efficiency of different TEM systems.

In case of 1-D models, the former problem has been largely resolved for conventional transverse electric (TE) and mixed TE and transverse magnetic (TE+TM) fields; thanks to the development of efficient quadrature algorithms for numerical evaluation of rapidly oscillating integrals (e.g. Anderson 1979; Tabarovsky and Sokolov 1982; Chave 1983; Goldman 1983, 1987). As a result, at present, the discussed limitation rarely affects a treatment of real data, which are normally measured to earlier times, but might be still a disturbing factor in theoretical analysis, when calculations are not limited by practically feasible times. The situation is much more severe in case of unimodal TM fields generated by vertical or circular electric dipole transmitters, which gained recently great popularity due to their exceptional sensitivity to electrically resistive targets such as hydrocarbons, gas hydrates and submarine fresh groundwater (e.g. Holten *et al*. 2009; Mogilatov, Zlobinskiy and Balashov 2017). At late times, these fields decay much faster than conventional TE and TE+TM ones and, as a result, their calculation using spectral methods becomes challenging also in a practically feasible time range.

The above mentioned direct time domain solutions represent the most universal and efficient way to overcome the late times calculation problems inherent to all spectral methods. Both approaches are discussed below in some greater details.

1.1 Spectral method

For the first time, the spectral method was developed and both analytically and numerically realized by Sheinman (1947) for two simple, but practically important geoelectric models of a conductive half space and a thin sheet (S-layer). By changing an order of integration in double Bessel–Fourier transforms, Sheinman (1947) analytically evaluated both integrals and obtained an elegant time domain solution in the form of exponential and special error and modified Bessel functions. In fact, his solutions and analysis have already consisted of all necessary elements for the development of a new geophysical method, but it took roughly two more decades, until the transient electromagnetic (TEM) method has been eventually developed in the former Soviet Union under the name 'Transient sounding method in the near zone' (Kaufman and Morozova 1970; Obukhov 1970) and was later on adopted in the West under the name 'Short offset transient electromagnetic (SHOTEM) or time domain electromagnetic') method. It should be noted that its far zone (long offset) modification (LOTEM) had been developed beforehand, but because it used switch on transmitter current, from geophysical point of view, it only represented some electromagnetic upgrade of the traditional direct current (DC) resistivity method.

Although, mathematically speaking, forward problems in SHOTEM and LOTEM are identical, they are fairly different from the computational point of view. Due to the slow decay of the LOTEM response at late times (DC in case of electric components), forward modelling algorithms in the LOTEM method are rather simple and they became available simultaneously with the theoretical and instrumental developments of the method in the early 1960s of the last century (Vanyan 1962). This was not the case with the SHOTEM method in general and with the forward modelling in particular. It took almost a decade after the LOTEM method has been developed, until geophysicists realized the unique feature of the SHOTEM method, which was available in no other structural geoelectric method, namely the ability of measuring pure secondary signals coming directly from the earth in the total absence of a parasitic primary field. Previously, the latter was mainly reduced by increasing the distance between transmitter and receiver and/or by applying different artificial compensation techniques. For the first time in the geophysical practice, the investigation depth was not controlled by the transmitter/receiver offset, but rather by the delay time after transmitter current has been switched off. This, in turn, led to the appearance of short offset and even zero-offset (combined or one-loop) arrays and, as a result, to significant increase in the lateral resolution of the method. It should be noted that similar to SHOTEM methodology, a method has been developed earlier in airborne mineral exploration, mainly for the search of highly conductive ore bodies (Barringer 1962).

Further analysis showed that, contrary to LOTEM, SHOTEM signals measured at sufficiently late times provide a very high sensitivity to geoelectric parameters of the earth (Kaufman and Keller 1983). However, due to a very fast decay with time and as a result an exceptional smallness of the signals, the late stage of the transient process represents instrumental and computational challenges for the SHOTEM method, particularly in the presence of highly resistive basement or sufficiently thick resistivity structures. Only with the development of digital recorders and sufficiently fast computers, it became a working method, first in the Soviet Union and then all over the world (e.g. Sidorov and Tikshaev 1969; McNeill 1980; Frischknect and Raab 1984; Macnae 1984). In mineral exploration, both modelling and interpretation at those times were based on entirely different models of confined conductors in free space and thus represented much lesser computational challenges than those considered below for one-dimensional (1-D) horizontally stratified Earth.

The very first 1-D multi-layered forward modelling software for the SHOTEM method has been developed at the beginning of the 1970s of the last century and it was solely based on the spectral method (e.g. Kaufman and Morozova 1970; Wait 1971; Anderson 1979). As a result, in this method the inevitable late-stage computational errors severely affected an efficiency of the interpretation, especially in case of an automatic inversion. During the next decade, various sophisticated numerical algorithms for treating the late-stage problem have been developed. Tabarovsky and Sokolov (1982) applied a spline-interpolation of the kernel function for an accurate, yet sufficiently fast numerical evaluation of the double Fourier–Bessel integrals (package named 'Alex'). Knight and Raiche (1982) derived the inverse Laplace transform to calculate 1-D transient response using the Gaver–Stehfast algorithm. Chave (1983) developed an algorithm, which integrates the product of the kernel and Bessel functions between the asymptotic zero crossings of the latter and sums the series of partial integrations using a continued fraction expansion. Similar approach can be applied to numerical evaluating Fourier integrals as well. One of the most accurate spectral algorithms is based on a deformation of the integration path of the inner Bessel integral into the complex plane of the integration variable, λ. By doing so, the oscillating Bessel function is transformed into exponentially damped Hankel function and the inner integral becomes numerically stable at any frequency (Goldman 1987). The outer Fourier integral is calculated along the real axis of ω and the calculations therefore still remain inaccurate at late times, albeit at later ones than those that used double oscillating integrals (see the comparison below).

These and some other algorithms allowed calculating TEM responses to fairly late times, which in most cases were sufficient for treating real data. However, irrespective of what specific spectral algorithm was used, the calculations always failed at sufficiently late times. The only difference between the specific codes was in the threshold time value, after which the calculations became inaccurate. The spectral method exhibits even more severe limitations in multi-dimensional modelling (e.g. Newman, Hohmann and Anderson 1986), due to the limited accuracy and number of frequencies obtained by calculating complicated three-dimensional integral equations in frequency domain.

It is important to emphasize that the discussed problem is inherent to all spectral codes and algorithms, because in a fixed-precision computing environment, it is difficult to accurately calculate rapidly oscillating Fourier–Bessel integrals with arbitrary parameters due to accumulating round-off errors and alternating signs, which cause severe cancellation issues.

1.2 Direct time domain methods

The above limitations are easily overcome by calculating transient fields directly in time domain. This can be done by different methods, namely:

1. By using finite-difference/finite element algorithms to numerically solve the appropriate boundary value problem (BVP) for time domain diffusion (heat conduction) equation. The method can be applied for both one-dimensional (1-D) and multi-dimensional models as well as for an arbitrary resistivity of the basement (e.g. Goldman 1983; Goldman and Stoyer 1983; Druskin and Knizhnerman 1988; Wang and Hohmann 1993). The obvious limitations of the method are the time-consuming algorithm and the lack of analytical asymptotic solutions.

2. By changing the order of integration in the Fourier–Bessel integrals followed by an analytical evaluation of the inner integral using the residue theorem (e.g. Goldman and Fitterman 1987). The method can be only applied to 1-D models above either insulating or ideally conducting basement, but calculations can be carried out for arbitrary resistivities by placing the basement deep enough. The solution was not obtained for an arbitrary number of layers.

3. By approximating the model by means of a set of S-layers, for which the analytical time domain solution is known (Epov and Yeltsov 1992; Tabarovsky and Epov 1998). The method

is limited by unimodal transverse electric fields generated by horizontal loops on the surface of layered Earth above an insulating basement.

4. By analytical solution of BVP for time domain diffusion (heat conduction) equation. This can be done by different methods. Historically, the first and the most commonly used one is the Tikhonov's method, which is based on separating variables (t and z) and reducing BVP to a Sturm–Liouville problem (Tikhonov 1946). The latter is solved as a series of eigenvalues, coefficients of which are analytically determined using initial conditions. Tikhonov (1950) also suggested another solution based on the so-called multiple reflection method that is particularly suitable at early times, when the former method is somewhat problematic. The Tikhonov's method was further expanded to a two-layered earth (Tikhonov and Skugarevskaya 1950) and was successfully applied to obtain multi-layered asymptotical solutions (Skugarevskaya 1959; Frolov 1965). All this, for conventional Tx–Rx configurations (horizontal electric and vertical magnetic dipoles). Further on, the method was also applied to obtain asymptotic solutions for non-conventional vertical electric dipole and circular electric dipole transmitters (Goldman and Mogilatov 1978; Mogilatov 1993) and for the development of the efficient multi-layered forward and inversion algorithms realized in the interpretation package named 'Podbor' (Mogilatov 2014). The latter exists in two versions, one named 'Podbor-S', which utilizes the spectral method and another termed 'Podbor-T', which applies the Tikhonov's algorithm. Because the algorithm is based on the use of a real arithmetic only, the package 'Podbor-T' was particularly feasible in the early 1990s of the last century, when computing facilities, which could be used in the field, were rather limited.

Although all direct time domain algorithms mentioned in (5) were based on the same Tikhonov's method, the latter could not be easily generalized for an arbitrary earth model energized by an arbitrary source. In this article, we describe the modification of the Tikhonov's method, which allows to obtain a solution for an arbitrary 1-D earth model energized by an arbitrary Tx–Rx array. This modification makes the Tikhonov's method being the most general and accurate technique for calculating transient fields and obtaining analytical late-stage asymptotic expressions compared to both the spectral method and all the above mentioned direct time domain solutions. To the best of our knowledge, such general Tikhonov's solution has never been published in English language, although some particular models and/or Tx–Rx configurations were considered in a number of articles (e.g. Pracser 1992; Mogilatov and Balashov 1996).

2 HORIZONTAL PLANE SOURCES

In order to distract from the consideration of specific horizontal sources such as current loop or vertical magnetic dipole (VMD), grounded line or horizontal electric dipole (HED) and circular electric line or dipole, let us represent an arbitrary horizontal Tx antenna by means of an extrinsic surface current density $j^{\text{ext}}(x,y)q(t)$ distributed on an arbitrary boundary (either real or fictitious) of a one-dimensional horizontally layered medium. This boundary can be the earth surface as well as any other horizontal plane located below or above it. Such a general presentation of transmitter antennae includes both standard electric and magnetic dipoles (or finite dimensional grounded lines and ungrounded current loops, respectively) as well as non-conventional arrays with distributed groundings. For example, the surface current density for major conventional sources, such as horizontal electric dipole (line), HED/HEL, and VMD (horizontal current loop), VMD/HCL, is represented as follows:

$$\begin{aligned} &\text{HEL} \rightarrow j_x^{\text{ext}}(x, y) = I\delta(y)[U(x + l/2) - U(x - l/2)], \\ &\text{HCL} \rightarrow j_r^{\text{ext}}(r) = I\delta(r - a), \end{aligned} \tag{1}$$

where I is a current in the source, $U(x)$ is the Heaviside step function, $\delta(x)$ is the Dirac delta-function, l is a length of HEL and a is a radius of HCL. It should be emphasized that the above presentation of the extrinsic current density differs from the common one, which considers the volume density having additional z-component (e.g. Everett 2013). The surface current density considered here has dimension A/m, which coincides with that of a magnetic field. It allows to obtain at once more universal solution for all conventional sources such as HED, VMD, grounded lines, final horizontal loops and even non-isolated wires or metallic sheets. Further details of the described presentation can be found in Mogilatov (1996).

Within each layer of the above model ($i = 0, 1, \ldots, N$), the sought electromagnetic field in a quasi-static approximation satisfies homogeneous system of Maxwell equations:

$$\begin{aligned} &\text{rot}\,\mathbf{H} = \sigma_i \mathbf{E}, \qquad \text{div}\,\mathbf{H} = 0, \\ &\text{rot}\,\mathbf{E} = -\mu_0 \tfrac{\partial \mathbf{H}}{\partial t}, \quad \text{div}\,\mathbf{E} = 0. \end{aligned} \tag{2}$$

The boundary conditions on all boundaries, but ($z = z_1$), are continuity of all horizontal components (H_x, H_y, E_x, E_y). On boundary ($z = z_1$), where the extrinsic surface current density is distributed (Fig. 1), special boundary conditions take place:

$$\begin{aligned} &[H_x]\big|_{z=z_l} = -j_y^{\text{ext}}(x, y)q(t),\ [E_x]\big|_{z=z_l} = 0, \\ &[H_y]\big|_{z=z_l} = j_x^{\text{ext}}(x, y)q(t),\ [E_y]\big|_{z=z_l} = 0. \end{aligned} \tag{3}$$

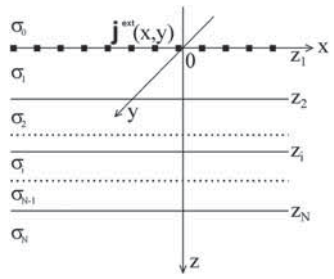

Figure 1 Model cross-section. As an example, the transmitter is located on the Earth surface.

It should be noted that the current waveform is defined here as a pulse of an arbitrary shape $q(t)$, which synchronously varies with time at all points of the surface current density distribution. The dimension of the latter (A/m) coincides with that of the magnetic field.

2.1 Separation of the field to transverse electric and transverse magnetic modes

The vector boundary value problem (BVP) (2) and (3) can be scalarized, if the horizontal electromagnetic components are expressed through the vertical ones. From equations (2), one obtains

$$\frac{\partial H_y}{\partial x} - \frac{\partial H_x}{\partial y} = \sigma_i E_z, \quad \frac{\partial H_x}{\partial x} + \frac{\partial H_y}{\partial y} = -\frac{\partial H_z}{\partial z}, \tag{4}$$

$$\frac{\partial E_y}{\partial x} - \frac{\partial E_x}{\partial y} = -\mu_0 \frac{\partial H_z}{\partial t}, \quad \frac{\partial E_x}{\partial x} + \frac{\partial E_y}{\partial y} = -\frac{\partial E_z}{\partial z}. \tag{5}$$

Let us now formulate BVP for E_z and H_z. In each layer, they must satisfy equation:

$$\Delta F = \mu_0 \sigma_i \frac{\partial F}{\partial t}, \quad F = E_z, H_z, \tag{6}$$

with boundary conditions at ($z = z_i$, $i = 1, 2, \ldots, N$) and taking into account (3):

$$\left[\frac{\partial E_z}{\partial z}\right]\Big|_{z_i} = 0,$$

$$[\sigma E_z]\big|_{z_i} = \left[\frac{\partial H_y}{\partial x} - \frac{\partial H_x}{\partial y}\right]\Big|_{z_i} = \begin{cases} \operatorname{div} \mathbf{j}^{\text{ext}} q(t), & i = l \\ 0, & i \neq l \end{cases}, \tag{7}$$

$$[\mu H_z]\big|_{z_i} = 0,$$

$$\left[\frac{\partial H_z}{\partial z}\right]\Big|_{z_i} = -\left[\frac{\partial H_x}{\partial x} + \frac{\partial H_y}{\partial y}\right]\Big|_{z_i} = \begin{cases} \operatorname{rot}_z \mathbf{j}^{\text{ext}} q(t), & i = l \\ 0, & i \neq l \end{cases}. \tag{8}$$

Thus, BVP for an arbitrary plane horizontal source is separated into two independent BVPs for scalar functions (H_z and E_z), which differently depend on a given distribution of the extrinsic current. We shall solve these problems by the method of separation of variables. Because the distribution of the extrinsic current density $j^{\text{ext}}(x,y)$ is arbitrary at the moment, let us use two-dimensional (2-D) Fourier transform with respect to the coordinates x and y:

$$f(x, y, z) = \frac{1}{(2\pi)^2} \int_{-\infty}^{\infty} \int_{-\infty}^{\infty} f^*(\xi, \eta, z) e^{i\xi x} e^{i\eta y} d\xi \, d\eta,$$

$$f^*(\xi, \eta, z) = \int_{-\infty}^{\infty} \int_{-\infty}^{\infty} f(x, y, z) e^{-i\xi x} e^{-i\eta y} dx dy. \tag{9}$$

Note that here we use the 2-D Fourier transform from considerations of generality. However, in case of a one-dimensional (1-D) earth model, the general 2-D Fourier transform for each specific current density distribution can be reduced to a 1-D Hankel (Bessel) transform.

By defining

$$E_z^*(z, t, \xi, \eta) = V(z, t, \lambda) D^*(\xi, \eta),$$

$$H_z^*(z, t, \xi, \eta) = X(z, t, \lambda) R^*(\xi, \eta), \tag{10}$$

where

$$D^* = \int_{-\infty}^{\infty} \int_{-\infty}^{\infty} \operatorname{div} \mathbf{j}^{\text{ext}}(x, y) e^{-i\xi x} e^{-i\eta y} dx dy,$$

$$R^* = \int_{-\infty}^{\infty} \int_{-\infty}^{\infty} \operatorname{rot}_z \mathbf{j}^{\text{ext}}(x, y) e^{-i\xi x} e^{-i\eta y} dx dy, \tag{11}$$

and functions V and X satisfy equation

$$F''_{zz} - (\xi^2 + \eta^2) F = \mu_0 \sigma_i \frac{\partial F}{\partial t}, \tag{12}$$

taking into account equations (4) and (5), we obtain the following expressions for the Fourier transforms of all components in each layer ($i = 0, 1, \ldots, N$):

$$\begin{aligned} H_x^* &= \bar{\eta}(\sigma_i V) D^* + \bar{\xi} X'_z R^*, & E_x^* &= \bar{\xi} V'_z D^* - \bar{\eta} \mu_0 \frac{\partial X}{\partial t} R^*, \\ H_y^* &= -\bar{\xi}(\sigma_i V) D^* + \bar{\eta} X'_z R^*, & E_y^* &= \bar{\eta} V'_z D^* - \bar{\xi} \mu_0 \frac{\partial X}{\partial t} R^*, \\ H_z^* &= X R^*, & E_z^* &= V D^*, \end{aligned} \tag{13}$$

where $\bar{\xi} = \frac{i\xi}{\lambda^2}$, $\bar{\eta} = \frac{i\eta}{\lambda^2}$, $\lambda^2 = \xi^2 + \eta^2$ and i is the imaginary unit. Functions X, X'_z and σV, V'_z are continuous on all source free boundaries.

Thus, a behaviour of the field is determined by two independent functions V and X, which generate E- and H-modes,

respectively. In other words, the transient process of an arbitrary source is a superposition of two different processes termed TM and TE (transversal magnetic and transversal electric, correspondingly). The contribution of each process is determined by coefficients D^* and R^*, which, according to equations (11), are related to the source of extrinsic currents by means of functions $\mathrm{div}\,\mathbf{j}^{\mathrm{ext}}(x, y)$ and $\mathrm{rot}_z\,\mathbf{j}^{\mathrm{ext}}(x, y)$. The former mode is determined by currents flowing into and out of electrodes (galvanic currents), whereas the latter mode is solely determined by eddy currents.

2.2 Solution of boundary value problem for functions, *V* and *X*

Functions, V and X can be determined by solving one-dimensional boundry value problem (BVP) either in frequency or in time domain. We will use Tikhonov's approach of solving the BVP in time domain (Tikhonov and Skugarevskaya 1950). First, we shall simplify the geoelectric model by considering both the upper and lower half spaces as insulators. Then, according to equation (12), the solutions for function $X(z,t)$ in these domains are

$$F(z,t) = F(z_1,t)\exp[\lambda(z-z_1)], \tag{14}$$

in the upper half space (air), and

$$F(z,t) = F(z_N,t)\exp[-\lambda(z-z_N)], \tag{15}$$

in the lowermost half space (basement).

Thus, the function domain for both X and V is limited along z by $z_1 \le z \le z_N$. At $z = z_1$ and $z = z_N$ function X is determined by the closing conditions connecting X and $\mathrm{d}X/\mathrm{d}z$ ($\mathrm{d}X/\mathrm{d}z = \pm\lambda X$), while function V equals 0. The BVP in question will be formulated using initial conditions at $t = 0$ for transmitter current switch off mode. Under the above conditions, the BVPs for functions X and V are formulated as follows:

Here, $\overline{X}(\lambda, z)$ and $\overline{V}(\lambda, z)$ are appropriate DC solutions. The former one is the Fourier transform of magnetic field of the DC extrinsic currents; the latter one is the Fourier transform of the currents flowing through the electrodes at $t = 0$. The current transmitter is located at one of the boundaries, $z = z_i$, $(i = 1, 2, \ldots, N)$ either real or fictitious. Both functions are infinitely small at $t \to \infty$.

The BVP (16) will be solved by separation of variables, in which X and V are sought as a superposition of solutions in the form of $A\zeta(z)\exp(-\alpha t)$, where $\mathrm{Re}\,\alpha \ge 0$. For function ζ, we obtain

$$\zeta''_{zz} - u_i^2\zeta = 0. \tag{17}$$

Here, $u_i^2 = \lambda^2 + k_i^2$, $k_i^2 = -\alpha\mu_0\sigma_i$, $(i = 0, 1, \ldots N)$. Function ζ in the ith layer can be expressed through its values on either lower or upper boundaries (within the layer). By designating $\zeta_i = \zeta(z_i)$ $(i = 1, 2, \ldots N)$, we obtain in each layer $(z_i \le z \le z_{i+1})$:

$$\zeta(z) = \zeta_i\cosh[u_i(z-z_i)] + \frac{\zeta_i'}{u_i}\sinh[u_i(z-z_i)], \tag{18}$$

where function $\zeta(z)$ is determined through its value on the upper boundary. The boundary conditions for X and V in (16) are formulated now for function ζ. The values of ζ_i and its derivative ζ_i' are determined successively from the upper boundary downwards setting $\zeta_1 = 1$ and satisfying the boundary conditions in (16). The conditions on the lower boundary $z = z_N$ represent the equations for determining α. The solution of these transcendental equations gives a set of discrete real values of $\alpha_j \ge 0$, which allows to represent the solution for X and V in the form of the real Fourier series:

$$\begin{Bmatrix} X \\ V \end{Bmatrix} = \sum_{j=0}^{\infty} C_j\zeta_j(z)T_j(t), \tag{19}$$

where

$T_j = -\int_{-\infty}^{t} q(\tau)\alpha_j \exp[-\alpha_j(t-\tau)]\mathrm{d}\tau$ for an arbitrary pulse current excitation and

a) function X	*b*) function V	
$X''_{zz} - \lambda^2 X = \mu_0\sigma_i\frac{\partial X}{\partial t}$,	$V''_{zz} - \lambda^2 V = \mu_0\sigma_i\frac{\partial V}{\partial t}$,	$z_i < z < z_{i+1}, i = 1, \ldots .N-1,$
$X'_z - \lambda X = 0,$	$V = 0,$	$z = z_1,$
$[X]\vert_{z=z_i} = 0,\ [X'_z]\big\vert_{z=z_i} = 0,$	$[\sigma V]\vert_{z=z_i} = 0,\ [V'_z]\big\vert_{z=z_i} = 0,$	$z = z_i$
$X'_z + \lambda X = 0,$	$V = 0,$	$z = z_N,$
$X = \overline{X}(\lambda, z),$	$V = \overline{V}(\lambda, z),$	$t = 0.$

(16)

$T_j = \exp(-\alpha_j t)$ for a step-off function used in the solution for all specific models and Tx–Rx arrays throughout the paper.

Coefficients C_j are determined as follows. Multiplying by ζ_k equation (19) for $t = 0$, and integrating the product along z within the function domain, we obtain

$$\int_{z_1}^{z_N} \zeta_k(z) \left\{ \begin{matrix} \overline{X}(z) \\ \overline{V}(z) \end{matrix} \right\} \mathrm{d}z = \sum_{j=0}^{\infty} C_j \int_{z_1}^{z_N} \zeta_j(z)\zeta_k(z)\mathrm{d}z. \tag{20}$$

The integrals in equations (20) are easily evaluated taking into account that $\overline{X}(\lambda, z)$ and $\overline{V}(\lambda, z)$ satisfy equation $F''_{zz} - \lambda^2 F = 0$ and the same boundary conditions as X and V, whereas ζ_j satisfies equation $\zeta''_{zz} - u_i^2\zeta = 0$. Then, one can see that $\mu_0\sqrt{\sigma}\zeta_j$ for X and $\sqrt{\mu_0}\sigma\zeta_j$ for V are orthogonal functions within $z_1 \le z \le z_N$, and we can determine C_j as follows:

$$\begin{matrix} a)\ \text{function}\ X & & b)\ \text{function}\ V \\ C_j = \dfrac{\zeta_{jl}}{\alpha_j\mu_0 \sum_{i=1}^{N-1} M_{ji}\sigma_i}, & & C_k = -\dfrac{\zeta'_{jl}}{\alpha_j\mu_0 \sum_{i=1}^{N-1} M_{ji}\sigma_i^2}, \end{matrix} \tag{21}$$

where, in each layer

$$M_{ji} = \int_{z_i}^{z_{i+1}} [\zeta_j(z)]^2\mathrm{d}z = \frac{1}{2u_{ji}^2}\left[(z_{i+1} - z_i)\left(\zeta_{ji}^2 u_{ji}^2 - [\zeta'_{ji}]^2\right) + \left(\zeta_{ji+1}\zeta'_{ji+1} - \zeta_{ji}\zeta'_i\right)\right]. \tag{22}$$

Note that $u_{ji} = \sqrt{\lambda^2 - \alpha_j\mu_0\sigma_i}$ might accept imaginary values. Then, the real hyperbolic equation (18) is transformed into the real trigonometric equation. It is worth mentioning that functions X and V are determined in the domain $z_1 \le z \le z_N$.

Now, let us apply the above general solutions to the specific Tx–Rx configurations.

2.3 Electric field of a horizontal circular current loop – unimodal transverse electric field

Due to the symmetry, there is a single component of the extrinsic surface current density, $j_\varphi^{\mathrm{ext}}(r)$, in a polar coordinate system. For the loop of a radius a, $j_\varphi^{\mathrm{ext}}(r) = I\delta(r - a)$. Then, in a cylindrical coordinate system one obtains

$$\mathrm{div}\,\mathbf{j}^{\mathrm{ext}} = \frac{1}{r}\frac{\partial(j_\varphi^{\mathrm{ext}})}{\partial\varphi} = 0, \mathrm{rot}_z\,\mathbf{j}^{\mathrm{ext}} = \frac{1}{r}\frac{\partial(r j_\varphi^{\mathrm{ext}})}{\partial r} = I[\delta(r - a)/r + \delta'(r - a)]. \tag{23}$$

For this array, $D^* = 0$ and the measured electric field is thus a unimodal transverse electric field. Making use of the axial symmetry and passing from Cartesian to cylindrical coordinates, one obtains the following Bessel (Hankel) transform instead of the original Fourier transform (12):

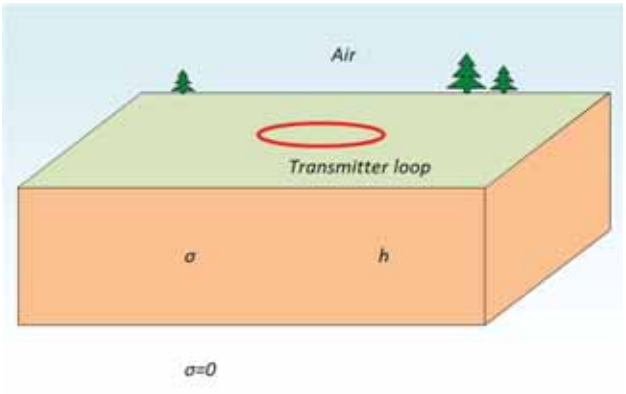

Figure 2 Horizontal circular transmitter loop on the surface of a two-layer earth with insulating basement.

$$R^* = 2\pi I\int_0^{\infty} [\delta(r - a)/r + \delta'(r - a)]J_0(\lambda r)r\,\mathrm{d}r = 2\pi I\lambda a J_1(\lambda a). \tag{24}$$

This allows to represent the required azimuthal electric field in the ith layer as follows:

$$E_\varphi(r, z, t) = \frac{M_z\mu_i}{\pi a}\int_0^{\infty} J_1(\lambda r)J_1(\lambda a)\lambda\frac{\partial X(z, t, \lambda)}{\partial t}\mathrm{d}\lambda, \tag{25}$$

where $M_z = I\pi a^2$ is a moment of the loop.

Contrary to the spectral method, in which the basic model is a homogeneous half space, in the Tikhonov's method such model is represented by a two-layer earth with insulating basement. Let us consider the solution for this model (Fig. 2).

Using the above described general Tikhonov's solution, one obtains for the basic model in question for the step-off current in the transmitter loop:

$$X(z, t) = \sum_{j=0}^{\infty} C_j\zeta_j(z)\exp(-\alpha_j t), \tag{26}$$

where

$$\zeta_j(z) = \frac{1}{\lambda}\cos(u_j z) + \frac{1}{u_j}\sin(u_j z), \quad 0 \le z \le h, \tag{27}$$

$u_j = \sqrt{\alpha_j\mu_0\sigma - \lambda^2}$, and for α_j we have the following equation:

$$\frac{\mathrm{tg}(u_j h)}{u_j} = -\frac{2\lambda}{u_j^2 + \lambda^2}, \tag{28}$$

and

$$C_j = -\frac{1}{\alpha_j \lambda M_j \mu_0 \sigma}, \quad M_j = \frac{h(u_j^2 + \lambda^2) + 2\lambda}{2u_j^2 \lambda^2}. \tag{29}$$

Substituting equations (26) into (25), one obtains:

$$E_\varphi = \frac{2M_z}{\pi a \sigma} \int_0^\infty \left\{ \sum_{j=0}^{\infty} \frac{u_j^2 \exp[-\alpha_j t + \lambda z}{h(u_j^2 + \lambda^2) + 2\lambda} \right\} J_1(\lambda r) J_1(\lambda a) \lambda \mathrm{d}\lambda. \tag{30}$$

Contrary to the double Hankel–Fourier integrals in the spectral method (e.g. Kaufman and Keller 1983), the latter equation allows to easily obtain an analytical late-stage asymptotic solution. Indeed, for $t \to \infty$, only small values of α_j contribute into equation (30). The latter take place at $j = 0$, that is for $\alpha_0 \approx \frac{2\lambda}{\mu_0 \sigma h}$ and $\lambda \to 0$. This leads to $M_0 \approx \sigma h$ and thus to much simpler integral expression for E_ϕ:

$$E_\varphi(r, t) \cong -\frac{I}{S} \int_0^\infty J_1(\lambda r) J_1(\lambda a) \lambda a \exp\left(\frac{-2\lambda t}{\mu_0 S}\right) \mathrm{d}\lambda, \tag{31}$$

where $S = \sigma h$ is a longitudinal conductance of the layer. The latter integral shows that the algorithm for calculating equation (30) is much more stable than that of the spectral method because the integrand exponentially decays with λ and the greater the time the faster the decay. In the spectral method, the mathematical convergence of the Fourier integral is only achieved by oscillating factor, thus leading to numerical instability and even to numerical divergence of the integral at sufficiently late times. The latter integral can be further simplified for later times by setting $J_1(\lambda a) \approx \lambda a/2$. Then it is evaluated analytically:

$$E_\varphi(t) = \frac{3M_z r}{\pi S} \frac{t}{\mu_0 S} \left[r^2 + \left(\frac{1}{\mu_0 S} \right)^2 \right]^{\frac{5}{2}} \cong \frac{3M_z r}{32\pi S} \left(\frac{t}{\mu_0 S} \right)^{-4}. \tag{32}$$

The former expression represents the field of a slab S that imitates a two layer earth at moderately late times. The latter expression represents the very late time asymptotic expression, which has been previously derived using the spectral method by much more complicated way (Kaufman and Keller 1983). It should be noted that the considered solution assumes an insulating basement. Kaufman and Keller (1983) obtained more general asymptotic expression for a slab resting on a finally resistive basement. The expression is simple, but mathematically is not strictly substantiated. Contrary, Singer and Green (2003) showed more complicated, but strictly substantiated asymptotic solution for the same model.

The opposite extreme case of the resistivity of the basement ($\rho_N = 0$) is less commonly used in the geophysical modelling. This is because of the two main reasons. First, such model adequately represents real earth, when the resistivity of the basement is less by two to three orders of magnitude than the average resistivity of the upper sequence. Such resistivity contrasts are not very common in geoelectric exploration. Second, the spectral method is suited to adequately treat the late time response of this model neither numerically nor analytically. Contrary, the described Tikhonov's method easily treats the solution for the model in question. In this case, the boundary condition on the lower boundary becomes $X = 0$, instead of the condition $X' + \lambda X = 0$ used above for the insulating basement. This means that for $\lambda = 0$, the appropriate eigenvalue equation does not have the zero solution. This, in turn, means that contrary to insulating or finally conducting basement, the response for the model in question exponentially decays at late times.

Let us consider the solution for two layer model in greater details. Then, instead of equation (30), we obtain

$$E_\phi(r, z, t) = -2I\rho \int_0^\infty J_1(\lambda r) J_1(\lambda a) \lambda a \left\{ \sum_{j=0}^{\infty} \frac{u_j^2 \exp(-\alpha_j t)}{\mu_0 S \alpha_j + \lambda} \right\} \mathrm{d}\lambda, \tag{33}$$

where α_j satisfies the following trigonometric equation:

$$\mathrm{tg}\left(h\sqrt{\mu_0 \alpha_j \sigma - \lambda^2}\right) = -\frac{\sqrt{\mu_0 \alpha_j \sigma - \lambda^2}}{\lambda}. \tag{34}$$

This equation has infinite number of solutions, none of which leading to $\alpha_j \to 0$ for $\lambda \to 0$.

This means that the field exponentially decays with time at very late stage. As a result, contrary to expectations, the late time apparent resistivity infinitely increases with time more steeply than they increase in the case of an insulating basement. This, in turn, causes the apparent resistivities for models with finitely conductive basement to form a phantom maximum, which might complicate the interpretation of real data, if the measurements are incomplete in time. This problem has been previously discussed by Goldman and Fitterman (1987), who had obtained exactly the same equations (30) and (33) using completely different method for solving boundary value problem.

2.4 Electric field of a circular electric dipole – unimodal transverse magnetic field

In order to define purely galvanic field, one must assign $R^* \equiv 0$, or for the entire plane $z = 0$ in the polar coordinate system:

$$\mathrm{rot}_z\,\mathbf{j}^{\mathrm{ext}} = \frac{1}{r}\left[\frac{\partial(r j_\varphi^{\mathrm{ext}})}{\partial r} - \frac{\partial(j_r^{\mathrm{ext}})}{\partial \varphi}\right] = 0. \quad (35)$$

The latter equation dictates an axially symmetric distribution of extrinsic currents, the density of which has only radial component, $j_r^{\mathrm{ext}}(r)$. In general, the dependence of r can be arbitrary, but let us start with the specific model in which the extrinsic current density is non-zero within a circle of radius, r_0, that is

$$j_r^{-\mathrm{ext}}(r) = \frac{I}{2\pi r}[U(r - r_0 + \mathrm{d}r_0/2) - U(r - r_0 - \mathrm{d}r_0/2)], \quad (36)$$

where $U(\mathrm{x})$ is the Heaviside function. Note that the current density synchronously varies with time, that is the time dependence is invariant with regard to r.

Such a configuration of the extrinsic current density provides unidirectional radial field excitation by the source, which is named the circular electric dipole (CED).

In order to obtain the solution for transient electromagnetic field excited by CED, let us consider first:

$$\begin{aligned}\mathrm{div}\,\mathbf{j}^{\mathrm{ext}} &= \frac{1}{r}\frac{\partial(r j_r^{\mathrm{ext}})}{\partial r} \\ &= \frac{I}{2\pi r}[\delta(r - r_0 + \mathrm{d}r_0/2) - \delta(r - r_0 - \mathrm{d}r_0/2)]. \quad (37)\end{aligned}$$

Thus, the divergence of the surface current density equals 0 everywhere, but along two concentric circles (grounding circles), where the divergence has infinite value.

For $\mathrm{d}r_0 / r_0 \to 0$, equation (37) is simplified and we obtain for the coefficient D^* (equation (11)):

$$D^*(\lambda) = 2\pi \int_0^\infty \mathrm{div}\,\mathbf{j}^{\mathrm{ext}} J_0(\lambda r) r\,\mathrm{d}r = I\mathrm{d}r_0 \lambda J_1(\lambda r_0). \quad (38)$$

Finally, we obtain the following equation for radial electric field within the ith layer of one-dimensional multi-layered earth in the cylindrical coordinate system:

$$E_r(r, z, t) = -\frac{I\mathrm{d}r_0}{2\pi}\int_0^\infty J_1(\lambda r) J_1(\lambda r_0)\frac{\partial V(z, t, \lambda)}{\partial z}\lambda \mathrm{d}\lambda. \quad (39)$$

It should be noted that the above considered transmitter dipole, CED, represents a physical idealization of a real source, which can be realized by finite-dimension radial wires grounded at a common centre ($a = 0$) and along the circle of radius, b (Fig. 3). In such case, the radial electric field, E_r, is obtained by integrating equation (39) along r_0:

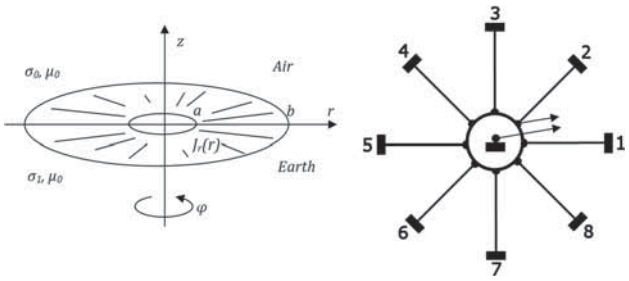

Figure 3 An 'ideal' (left) and 'real' (eight legs) CEDs.

$$E_r(r, z, t) = \frac{I}{2\pi}\int_0^\infty J_1(\lambda r)[J_0(\lambda b) - J_0(\lambda a)] \frac{\partial V(z, t, \lambda)}{\partial z}\mathrm{d}\lambda. \quad (40)$$

More detailed theoretical description and practical examples of the CED method are given by Mogilatov (1996, 2014) and by Mogilatov *et al.* (2017).

As an example, let us determine the CED field for the model shown in Fig. 2. Applying the above described Tikhonov's algorithm, the solution for the transient field induced in the ground after switch off current I in CED is sought in the form (19):

$$V(z,\ t) = \sum_{j=0}^{\infty} C_j \zeta_j(z)\exp(-\alpha_j t), \quad (41)$$

where applying the boundary condition $\zeta'_{j1} = 1$ in the upper boundary, one obtains

$$\zeta_j(z) = \frac{\sin(u_j z)}{u_j}, \quad 0 \le z \le h. \quad (42)$$

Here, $u_j = \sqrt{\alpha_j \mu_0 \sigma - \lambda^2}$ and applying the boundary condition in the lower boundary,

$\sin(u_j h) = 0$, one obtains

$$u_j = j\frac{\pi}{h},\ \alpha_j = \frac{1}{\mu\sigma}\left[\left(j\frac{\pi}{h}\right)^2 + \lambda^2\right],\ C_j = -\frac{2j\pi}{(j^2\pi^2 + \lambda^2 h^2)\sigma}. \quad (43)$$

Finally, we obtain the expression for V everywhere within the first layer:

$$V(z, t) = -\frac{2\pi}{\sigma}\sum_{j=1}^{\infty}\frac{j}{j^2\pi^2 + \lambda^2 h^2}\sin\left(\frac{j\pi}{h}z\right) \exp\left[-\frac{t(j^2\pi^2 + \lambda^2 h^2)}{\mu_0 \sigma h^2}\right]. \quad (44)$$

And for all components of the electromagnetic field:

$$H_\varphi(r,z,t) = -\frac{I}{2\pi}\int_0^\infty J_1(\lambda r)[J_0(\lambda b)-1][\sigma V(z,t,\lambda)]\mathrm{d}\lambda,$$
$$E_r(r,z,t) = -\frac{I}{2\pi}\int_0^\infty J_1(\lambda r)[J_0(\lambda b)-1]\frac{\partial V(z,t,\lambda)}{\partial z}\mathrm{d}\lambda,$$
$$E_z(r,z,t) = -\frac{I}{2\pi}\int_0^\infty J_0(\lambda r)[J_0(\lambda b)-1]V(z,t,\lambda)\lambda\mathrm{d}\lambda. \quad (45)$$

It is clear that at sufficiently late times only the first term in series (44) with $\lambda \to 0$ contributes to the total field. Therefore, the late-stage asymptotic, for example radial electric field, takes the form:

$$E_r(t) \cong \frac{Ib^2 r}{4\pi\sigma h^5}\left(\frac{\sigma\mu_0 h^2}{2t}\right)^2 \exp\left(-\frac{\pi^2 t}{\sigma\mu_0 h^2}\right). \quad (46)$$

The latter result describes an exceptional feature of the transverse magnetic (TM) field as compared to conventional transverse electric (TE) and mixed TE–TM processes. Only TM fields exponentially decay at late times in presence of a horizontally layered earth above an insulating basement and depend on all geoelectric parameters of the earth separately instead of just a total longitudinal conductance as conventional methods do. Such behaviour leads to extremely high (theoretically unlimited) resolving power of the CED method. Another unique feature of the TM fields is the total absence of magnetic field in the air and the earth surface. Thanks to this feature, the CED method becomes particularly sensitive to any lateral resistivity variations and this phenomenon was successfully realized in the vertical electric current sounding method (Mogilatov 1996; Mogilatov *et al.* 2017).

3 VERTICAL ELECTRIC LINE/DIPOLE

In the previous section, we considered the Tikhonov's solution of the time domain boundary value problem for the layered earth energized by arbitrary extrinsic currents having only horizontal components. In this section, we shall consider the appropriate solution for the same model but energized by only vertical extrinsic currents. The latter are represented by well-known, but still not so widely used vertical electric lines or dipoles. Formally, this transmitter was first introduced in time domain by Nazarenko (1961), but its remarkable features were recognized and theoretically investigated using the above mentioned Tikhonov's method only more than two decades afterwards (Goldman and Mogilatov 1978). Due to the difficulties in practical application of strictly vertical transmitter lines the method was abandoned for another three decades, until it was successfully applied for the marine hydrocarbon exploration by Holten *et al.* (2009). Since then, the vertical electric dipole (line) method was extensively investigated both theoretically (e.g. Um *et al.* 2012; Singer and Artamonova 2013; Goldman *et al.* 2015; Barsukov and Fainberg 2017) and practically (e.g. Helwig *et al.* 2013).

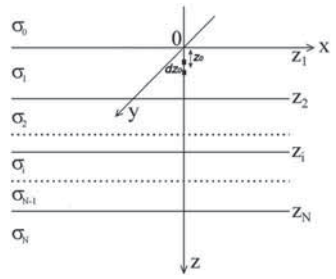

Figure 4 Vertical electric dipole (VED) in the first layer of an arbitrary horizontally layered earth.

3.1 The general solution

Let us consider an arbitrary horizonally layered model, in which all layers are isotropic and non-magnetic. Vertical electric dipole (VED) is located on z-axis at point $z = z_0$ of an arbitrary layer including the upper and lower half spaces (Fig. 4). The moment of VED is defined as $I_z(t) = I\mathrm{d}z_0 q(t)$, where I is a current.

The Maxwell's equations for all non-zero field components (E_r, E_z and H_φ) in each layer are presented in cylindrical coordinate system as follows:

$$-\frac{\partial H_\varphi}{\partial z} = \sigma E_r, \quad \frac{1}{r}\frac{\partial(rH_\varphi)}{\partial r} = \sigma E_z,$$
$$\frac{\partial E_r}{\partial z} - \frac{\partial E_z}{\partial r} = -\mu_0 \dot{H}_\varphi, \quad \frac{1}{r}\frac{\partial(rE_r)}{\partial r} + \frac{\partial E_z}{\partial z} = 0. \quad (47)$$

By separating variables and satisfying all the above mentioned conditions, the solution for the components can be presented in the form:

$$E_r = -\frac{I\mathrm{d}z_0}{4\pi}\int_0^\infty J_1(\lambda r)\lambda V'_z(z,t,\lambda)\mathrm{d}\lambda,$$
$$E_z = -\frac{I\mathrm{d}z_0}{4\pi}\int_0^\infty J_0(\lambda r)\lambda^2 V(z,t,\lambda)\mathrm{d}\lambda,$$
$$H_\varphi = \frac{I\mathrm{d}z_0}{4\pi}\int_0^\infty J_1(\lambda r)\lambda(\sigma V)\mathrm{d}\lambda. \quad (48)$$

The presence of VED can be taken into account by neglecting the influence of the medium in the immediate vicinity of the source. Then, the magnetic field is determined using the Biot–Savart law as follows:

$$H_\varphi = \frac{I\mathrm{d}z_0 q(t)}{4\pi}\frac{r}{R^3} \equiv \frac{I\mathrm{d}z_0 q(t)}{4\pi}\int_0^\infty J_1(\lambda r)\lambda\exp(-\lambda|z|)\mathrm{d}\lambda. \quad (49)$$

Comparing the latter expression with the appropriate one in (48) for $z \to z_0$, one obtains $\sigma V \to \exp(-\lambda|z|)\, q(t)$. This means that the vertical derivative $\mathrm{d}(\sigma V)/\mathrm{d}z$ is discontinuous at point z_0 with the discontinuity leap of $2\lambda q(t)$. Thus, one obtains the following boundary value problem (BVP) for function V:

$$\begin{aligned}
&\frac{\partial^2 V}{\partial z^2} - \lambda^2 V = \mu_0 \sigma_i \frac{\partial V}{\partial t} \quad - \text{in each layer},\\
&[\sigma V]|_{z=z_i} = 0,\ [V'_z]\big|_{z=z_i} = 0,\\
&[\sigma V]|_{z=z_0} = 0,\ [\sigma V'_z]\big|_{z=z_0} = 2\lambda q(t),\\
&V \to 0, |z| \to \infty,\\
&V \to 0, t \to \infty,\ \text{if } q(t) = 0 (t > T).
\end{aligned} \tag{50}$$

The solution to BVP (50) will be sought by the Tikhonov's method. Considering a quasi-static approximation and letting zero conductivity to the upper and lower half spaces, instead of the BVP (50), which is defined in the domain $-\infty \le z \le \infty$, one obtains an appropriate BVP within the bounded domain $z_1 \le z \le z_N$. If the transmitter current is switched off at $t = 0 (q(t) = 1 - U(t)$, where $U(t)$ is the Heaviside function), the BVP in question can be splitted into two independent problems, namely the quasi-static one without a source and the DC solution for VED. Thus, instead of (50) we obtain:

$$\begin{aligned}
&V''_{zz} - \lambda^2 V = \mu_0 \sigma_i \frac{\partial V}{\partial t}, z_i \le z \le z_{i+1}, (i = 1, \dots N-1),\\
&V = 0,\ z = z_1,\\
&[\sigma V]|_{z=z_i} = 0,\ [V'_z]\big|_{z=z_i} = 0, i = 2, \dots . N-1,\\
&V = 0, z = z_N,\\
&V = \overline{V}(\lambda, z), t = 0,\\
&V = 0, t = \infty,
\end{aligned} \tag{51}$$

where $\overline{V}(\lambda, z)$ is the DC solution. Separating the variables, one obtains the solution for V as a series:

$$V = \sum_{j=0}^{\infty} C_j \zeta_j(z) \exp(-\alpha_j t). \tag{52}$$

Functions ζ_j satisfy the following Sturm–Liouville problem:

$$\begin{aligned}
&\zeta''_{jzz} - u_{ji}^2 \zeta_j = 0, \quad z_i \le z \le z_{i+1}, (i = 1, \dots, N-1),\\
&\zeta_j = 0, z = z_1,\\
&[\sigma \zeta_j]\big|_{z=z_i} = 0,\ [\zeta'_{jz}]\big|_{z=z_i} = 0, \quad i = 2, \dots, N-1,\\
&\zeta_j = 0, \quad z = z_N,
\end{aligned} \tag{53}$$

where $u_{ji}^2 = \lambda^2 - \alpha_j \mu_0 \sigma_i$.

According to equation (53), ζ_j has the following solution in the ith layer:

$$\zeta_j(z) = A_i \exp(u_{ji} z) + B_i \exp(-u_{ji} z), \tag{54}$$

where A_i and B_i can be expressed through the values of the function and its first vertical derivative on the upper and lower boundaries of the appropriate layer. Designating $\zeta_{ij} = \zeta_j(z_i),\ \zeta'_{ji} = \zeta'_{jz}(z_i),\ (i = 1,\ 2, \dots N)$, one obtains in each layer ($z_i \le z \le z_{i+1}, i = 1, 2, \dots N-1$):

$$\zeta_j(z) = \zeta_{ji} \cosh[u_{ji}(z - z_i)] + \frac{\zeta'_{ji}}{u_{ji}} \sinh[u_{ji}(z - z_i)]. \tag{55}$$

Thus, eq. (55) represents a recurrent algorithm for the solution in the entire domain $z_1 \le z \le z_N$. According to BVP (33),…., $\zeta_{j1} = 0$ and $\zeta'_{j1} = \lambda$. Then, ζ_j is successively determined from the upper boundary downwards using the recurrent solution (55) and satisfying the boundary conditions (53). The condition on the lower boundary represents an equation for determining eigenvalues, α_j. As a matter of fact, the solution to BVP (53) can be characterized as a classical eigenfunctions and eigenvalues problem with all real eigenvalues, which can be arranged in the form of an indefinitely increasing monotone sequence ($\alpha_0 < \alpha_1 < s < \alpha_j < s$) (e.g. Kamke 1977). The eigenfunctions are orthogonal functions that can be seen from consideration of their antiderivatives:

$$\begin{aligned}
&\int \zeta_j \zeta_k \mathrm{d}z = \frac{1}{(\alpha_k - \alpha_j)\mu_0 \sigma} (\zeta'_j \zeta_k - \zeta_j \zeta'_k),\\
&\int \zeta_j^2 \mathrm{d}z = \frac{1}{2u_j^2} \left\{ z \left[u_j^2 \zeta_i^2 + (\zeta'_j)^2 \right] - \zeta'_j \zeta_j \right\}.
\end{aligned} \tag{56}$$

Multiplying each function ζ_j by $\sqrt{\mu_0}\sigma$, one obtains a set of orthogonal functions in the domain $z_1 \le z \le z_N$. Coefficients C_j are determined by satisfying the initial condition for function V (equation (52) for $t = 0$) and using the orthogonality of functions $\sqrt{\mu_0}\sigma \zeta_j$ in the domain $z_1 \le z \le z_N$. Thus,

$$C_j = \frac{\int_{z_1}^{z_N} \mu_0 \sigma^2(z) \overline{V}(z) \zeta_j(z) \mathrm{d}z}{\int_{z_1}^{z_N} \mu_0 \sigma^2(z) \zeta_j^2(z) \mathrm{d}z}, \tag{57}$$

or taking into account the conditions for function $\overline{V}(\lambda, z)$ and antiderivative

$$\int \overline{V} \zeta_j \mathrm{d}z = \frac{1}{\alpha_j \mu_0 \sigma} (\overline{V}' \zeta_j - \overline{V} \zeta'_j), \tag{58}$$

we finally obtain

$$C_j = \frac{2\lambda \zeta_j(z_0)}{\alpha_j \sum_{i=1}^{N-1} M_{ji} \mu_0 \sigma_i^2}, \tag{59}$$

where in each layer

$$M_{ji} = \int_{z_i}^{z_{i+1}} [\zeta_j(z)]^2 \mathrm{d}z = \frac{1}{2u_{ji}^2}\left[(z_{i+1} - z_i)\left(\zeta_{ji}^2 u_{ji}^2 - [\zeta'_{ji}]^2\right) + \left(\zeta_{ji+1}\zeta'_{ji+1} - \zeta_{ji}\zeta'_{ji}\right)\right]. \quad (60)$$

3.2 Two-layer model

In conclusion, let us consider as an example the simplest canonical model of a two layered earth with insulating basement (Fig. 2). Using the general solution (48), for example radial electric field, one obtains for the two-layer model:

$$E_r = -\frac{I\mathrm{d}z_0}{4\pi}\int_0^\infty J_1(\lambda r)\lambda V'_z(z,\, t,\, \lambda)\mathrm{d}\lambda, \quad (61)$$

where

$$V(z,\, t,\, \lambda) = \frac{4\lambda}{h\mu_0\sigma^2}\sum_{j=0}^{\infty}\frac{\sin(u_j z)\sin(u_j z_0)}{\alpha_j}\exp(-\alpha_j t), \quad (62)$$

$u_j = \sqrt{\alpha_j\mu_0\sigma - \lambda^2}$ and α_j are the solutions of the trigonometric equation $\sin(u_j h) = 0$:

$$\alpha_j = \left(\frac{j^2\pi^2}{h^2} + \lambda^2\right)\frac{1}{\mu_0\sigma}, \quad j = 1,\, 2,\, 3, \ldots \quad . \quad (63)$$

Due to the exponential decay of the kernel function in equation (61), the numerical Bessel (Hankel) integral converges very fast and in the later time it converges faster. Indeed, for $t \to \infty$, the series (62) is determined by the first term at $\lambda \to 0$. This leads to the following late-stage asymptotic expression:

$$E_r(t) \cong \frac{Idz_0 r}{\pi^2\sigma h^4}\sin\left(\frac{\pi z_0}{h}\right)\left(\frac{\sigma\mu_0 h^2}{2t}\right)^2\exp\left(-\frac{\pi^2 t}{\sigma\mu_0 h^2}\right). \quad (64)$$

Similarly to the above considered circular electric dipole (CED) (equation (46)), the field of vertical electric dipole (VED) also exponentially decays at late times and separately depends on conductivity and thickness of the layer. Such dependence provides superior detectability and vertical resolution of both VED and CED compared to all conventional geoelectric and geoelectromagnetic method in DC, frequency and time domains. Analysis shows that similar behaviour of the VED/CED fields holds in an arbitrary horizontally layered earth above an insulating or ideally conducting basement. The fields exponentially decay at late times and separately depend on all geoelectric parameters of the model.

Comparison of equations (46) and (64) shows that the field of a shallow VED ($z_0 << h$), coincides with that of a surface CED, if $Ib^2/4 = Idz_0 z_0$, where b is the radius of CED. This relationship keeps at all times and in an arbitrary earth model. Thus, CED is in fact a surface analogue of a shallow VED. If they both are immersed within a conductive earth, their fields become different, because CED is a quadrupole everywhere and VED is a dipole within the earth and a quadrupole near the earth–air boundary (Wait 1997). However, because both sources generate unimodal TM fields, their behaviour is similar for any location within the earth and identical, when they are located near the earth surface.

4 DIRECT TIME DOMAIN SOLUTION FOR THE FOURIER–HANKEL INTEGRALS

The above described Tikhonov's method is not the only method to obtain the solution directly in time domain. Using canonical Fourier–Besel (Hankel) transforms in the spectral method and changing the order of integration, one can convert the inner Fourier integral to Fourier series, which is identical to that one obtained by the Tikhonov's method. Such conversion is only possible over insulating or ideally conducting basement, because these are the models in which the inner integrand has poles in the complex plane of the integration variable, ω. This in turn allows to apply the residue theorem and thus to evaluate the Fourier integral in the form of rapidly converging Fourier series directly in time domain. Goldman and Fitterman (1987) applied this approach to calculating unimodal transverse electric (TE) field ($\mathrm{d}B_z/\mathrm{d}t$) of a horizontal loop. Below, we consider similar solution for unimodal transverse magnetic (TM) field (E_r) generated by a circular electric dipole (CED) on the surface of a two-layer earth with an insulating basement (Fig. 2).

The spectral solution for this model can be represented as follows (Mogilatov and Balashov 1996; Mogilatov 2014):

$$E_r(t) = \frac{1}{2\pi}\int_{-\infty}^{\infty}\frac{1}{-\mathrm{i}\omega}E_r(\omega)\mathrm{e}^{-\mathrm{i}\omega t}\mathrm{d}\omega, \quad (65)$$

$$E_r(z,\omega,\lambda) = \frac{I}{2\pi}\int_0^\infty \mathrm{J}_1(\lambda r)[J_0(\lambda b) - 1]\frac{\partial V(z,\omega,\lambda)}{\partial z}d\lambda. \quad (66)$$

On the earth's surface ($z = 0$)

$$\frac{\partial V(\omega,\lambda)}{\partial z} = \frac{p}{\sigma}\frac{\cosh(ph)}{\sinh(ph)}, \quad (67)$$

where $p = \sqrt{\lambda^2 - \mathrm{i}\omega\mu_0\sigma}$.

Let us change the order of integration in (65) and (66) and consider the inner Fourier integral

$$S(t,\lambda)=\frac{1}{2\pi\sigma}\int_{-\infty}^{\infty}\frac{p}{-\mathrm{i}\omega}\frac{\cosh(ph)}{\sinh(ph)}\mathrm{e}^{-\mathrm{i}\omega t}\mathrm{d}\omega, \tag{68}$$

which represents a part of a contour integral including the entire axis of ω and an arc of infinite radius, where the integral equals 0. Then, according to the residue theorem (e.g. Korn and Korn 1968), one obtains:

$$\int_C f(\omega)\mathrm{d}\omega=2\pi\mathrm{i}\sum_{j=1}^{n}\mathrm{Res}\ f(a_j), \tag{69}$$

where a_j are the poles of the integrand.

$$S(t,\lambda)=-\frac{1}{\sigma}\sum_{j=1}^{n}\mathrm{Res}\left[\frac{p_j}{a_j}\frac{\cosh(p_jh)}{\sinh(p_jh)}\mathrm{e}^{-\mathrm{i}a_jt}\right], \tag{70}$$

where $p_j=\sqrt{\lambda^2-\mathrm{i}a_j\mu_0\sigma}$. It is clear that the poles are located at points, where hyperbolic sine becomes trigonometric one, that is at $ph=\mathrm{i}x$, where x is real number. Setting $\sin(ph)=0$, we obtain the following equation for the poles

$$a_j=-\frac{\mathrm{i}}{\mu_0\sigma}\left(\frac{j^2\pi^2}{h^2}+\lambda^2\right),\quad j=1,2,3,\ldots. \tag{71}$$

If $f(\omega)=g(\omega)/q(\omega)$, then Res $f(a_j)=g(a_j)/q'(a_j)$. Using this well-known feature and taking the derivative of $\sinh(ph)$ with respect to a, we obtain:

$$S(t,\lambda)=-\frac{1}{\sigma}\sum_{j=1}^{\infty}\mathrm{Res}\left[\frac{p_j}{a_j}\frac{\cosh(p_jh)}{\sinh(p_jh)}\mathrm{e}^{-\mathrm{i}a_jt}\right]=$$
$$-\frac{2}{\mu_0\sigma^2h}\sum_{j=1}^{\infty}\frac{(\lambda^2-\mathrm{i}a_j\mu_0\sigma)}{\mathrm{i}a_j}\mathrm{e}^{-\mathrm{i}a_jt}. \tag{72}$$

Or

$$S(t,\lambda)=-\frac{2}{\sigma h}\sum_{j=1}^{\infty}\frac{j^2\pi^2}{(j^2\pi^2+\lambda^2h^2)}\exp\left[-\frac{t(j^2\pi^2+\lambda^2h^2)}{\mu_0\sigma h^2}\right]. \tag{73}$$

Finally, we obtain the following equation for the radial electric field of VED on the earth surface.

$$E_r(r,t)=-\frac{I}{2\pi}\int_0^{\infty}J_1(\lambda r)[J_0(\lambda b)-1]S(t,\lambda)\mathrm{d}\lambda. \tag{74}$$

This expression is identical to that one obtained above by the Tikhonov's method (equation (45) with $z=0$).

Calculations show that the faster a transient response decays at late times the less accurate is spectral method using numerical Fourier–Hankel transforms along real axes of integration variables. The reason for this phenomenon is quite clear: the resulting small numbers are obtained by summation of rapidly oscillating integrands. Although the accuracy of the method strongly depends on the specific computational algorithm used, there is always some threshold measurement time, after which any spectral algorithm fails to accurately calculate the transient response (e.g. Goldman 1983). At present, there are several sophisticated spectral algorithms, which allow accurate calculations of the unimodal TE and mixed TE–TM fields in the entire practical time range. However, even these most accurate algorithms turned out inefficient in calculating unimodal TM fields in presence of very high resistivity (theoretically insulating) structures. At the same time, the above described Tikhonov's method in most cases provides sufficiently accurate results at late times for all field types.

Figure 5(a,b) shows transient responses of a central loop array located on the surface of a two-layered earth with insulating basement. The model is shown in Fig. 2 with the receiver coil located in the centre of the loop. The responses are calculated by four different spectral algorithms and by the above described Tikhonov's method. The rigorous responses are accompanied by the late-stage asymptotic calculations using equation (32) slightly modified for the central loop array. For greater visual clarity, the responses normalized by the late-stage asymptotic values are presented in Fig. 5(b), in addition to absolute values shown in Fig. 5(a).

Comparison of the responses calculated by spectral methods shows that at sufficiently late times all of them deviate from each other and from the late-stage asymptotic response. The threshold times, after which the considered spectral codes become inaccurate, are presented in Table 1.

Among all the considered spectral algorithms, the most accurate is that one which calculates the inner Bessel integral by deformation of the integration path into the complex plane of the integration variable, λ (code Podbor-S). It gradually deviates from the Tikhonov's calculations and the late-stage asymptotic formula at approximately 300 ms. Taking into account that in the considered model all geoelectric parameters could be resolved at approximately 30 ms, when the right ascending branch of the late-stage apparent resistivity curve exceeds by approximately 30% its minimum value, all considered algorithms are accurate far beyond the practically required limits. This is not the case for much faster damping TM fields, though.

Let us consider the same model as in the previous example, which is energized by an ideal CED transmitter shown in Fig. 3 (left). The radius of CED is 100 m and the response is picked up by a small radial electric dipole at a distance (offset) of 200 m. Again, the calculations are carried by the same three methods, namely, spectral method, Tikhonov's method

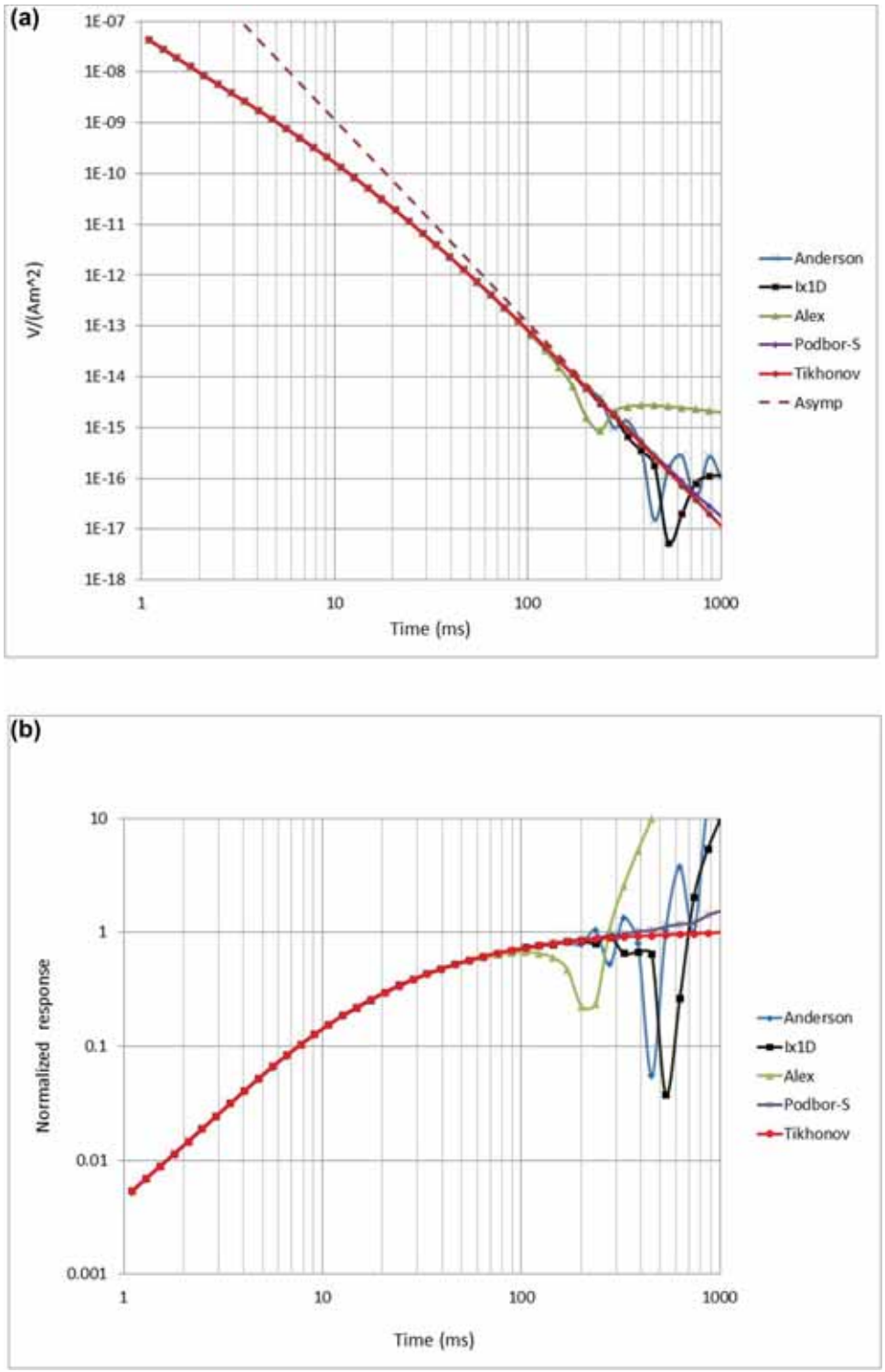

Figure 5 Central loop TE-responses calculated using Tikhonov's and four different spectral algorithms explained in Table 1: (a) absolute values in V/(Am^2) and (b) the responses normalized by the late stage asymptotic formula (32). The model is shown in Fig. 2 for $\sigma = 0.05$ S/m, h = 400 m and the Tx radius ≈55.8 m (equivalent to 100 by 100 m square loop). The threshold time values, starting from which spectral algorithms fail, are listed in Table 1.

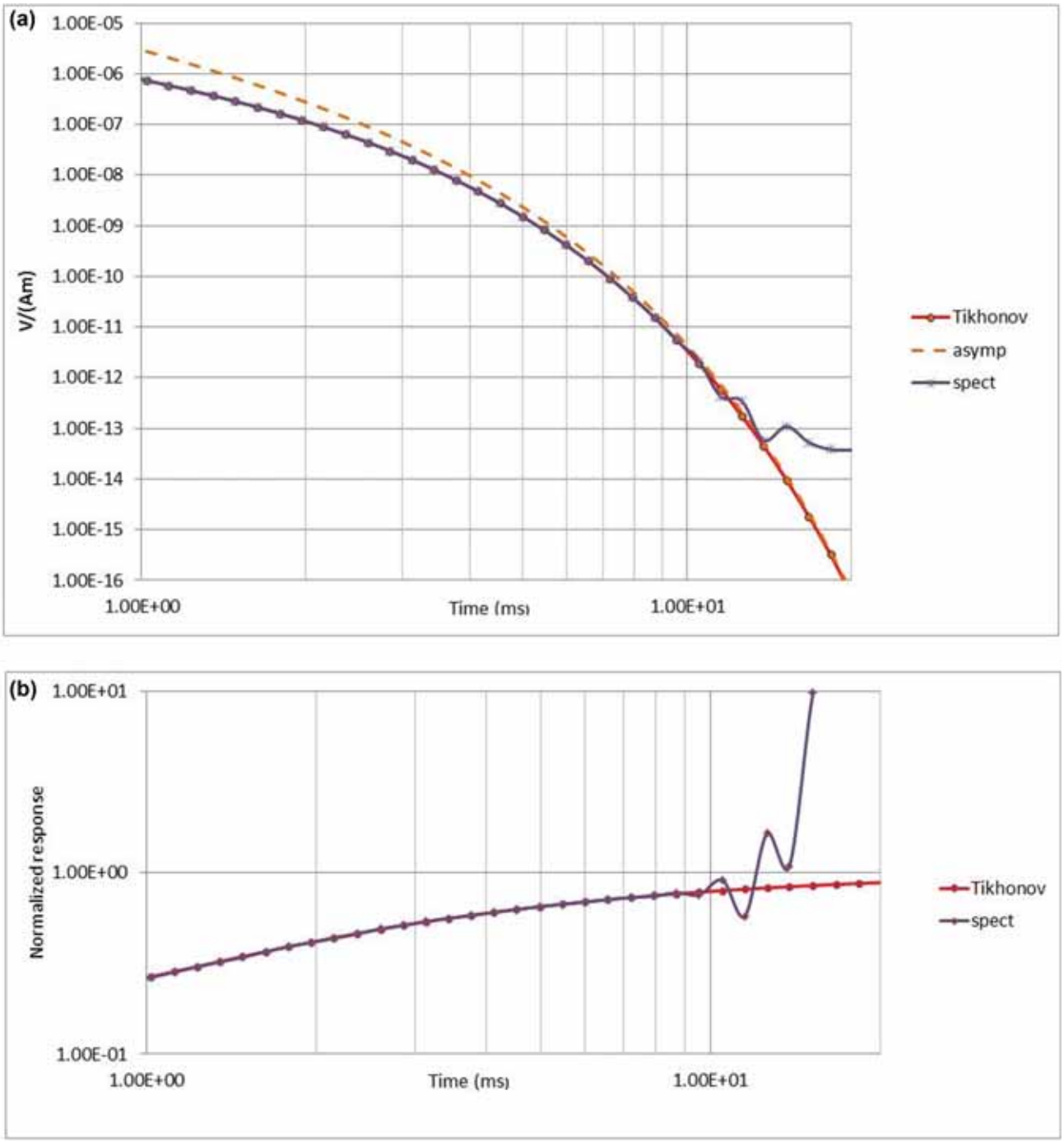

Figure 6 Radial electric field of CED calculated using Tikhonov's and the most accurate spectral algorithm shown in Fig. 5 (Podbor-S): (a) absolute values in V/(Am) and (b) the responses normalized by the late stage asymptotic formula (46). The model is the same as shown in Fig. 2 for $\sigma = 0.05$ S/m, h = 400 m and the CED radius = 100 m and the Rx offset = 200 m.

Table 1 Spectral algorithms and codes used to calculate responses in Fig. 5

Code Name	Threshold Time (ms)	Algorithm
Alex	90	The inner Bessel integral is spline interpolated between different frequencies. Filon's method (1930) is used for the numerical Fourier transform.
Anderson	190	The inner Bessel integral is calculated using Anderson's adaptive digital filtering. Filon's method (1930) is used for the numerical Fourier transform.
Ix1D v3	250	Anderson's style digital filtering is used for both numerical Bessel and Fourier transforms (Interpex, 1983, http://www.interpex.com/ix1dv3/ix1dv3.htm).
Podbor-S	300	The integration path of the inner Bessel integral is properly deformed into the complex plane, where the oscillating Bessel function is transformed into the rapidly damped Hankel function. Filon's method (1930) is used for the numerical Fourier transform.

and late-stage asymptotic solution (equation (46)). However, this time only one spectral algorithm realized in the Podbor-S code is examined. This is because it was shown in the previous example that among all tested spectral algorithms Podbor-S provides the most accurate results. Besides, no other spectral codes for calculating TM fields are presently available. The calculations are shown in Fig. 6(a,b) in exactly the same formats as those in Fig. 5(a,b) for the TE field.

Comparison of the three methods clearly shows that the most accurate algorithm among considered four spectral algorithms fails starting from approximately 10 ms. Although it is generally possible that even more accurate spectral codes will be developed in future, no significant gain in the measurement time could be achieved due to extremely fast, nearly exponential decay of the TM response at late times (equation (46)). This means that, contrary to TE and TE+TM fields, the use of the spectral method for calculating TM fields could be limited not only in theoretical studies, but also in the interpretation of real field data.

4.1 Modelling the 'real' circular electric dipole response

Because the above discussed 'ideal' circular electric dipole (CED) cannot be realized in practice, the question arises of what would be a sufficient amount of radial electric dipoles, which adequately represent an 'ideal' CED? Both calculations and field measurements show that eight symmetrical dipoles as shown in Fig. 3 (right) are enough to provide the response, which practically coincides with that of an 'ideal' CED (e.g. Mogilatov 1996, 2014). Adding more pairs of symmetrical dipoles alters the total response by less than 1%. Does it mean that modelling of 'real' CED can be carried out by using well-developed algorithms for calculating fields of electric dipoles? The answer is strictly negative, at least, if the model consists of highly resistive layers or rests on a high resistivity basement. In such models, the field of horizontal electric dipoles decays at late times as a power of time, whereas the field of CED damps exponentially (equation (46)). It is quite clear that irrespective to the accuracy of calculations of the individual electric dipole responses, there will be always a time instant, after which the sum of the individual responses will produce a large error caused by a subtraction of relatively large transverse electric components, which are absent in the resulting unimodal transverse magnetic field of CED.

Let us illustrate these qualitative considerations by a numerical example. Table 2 exhibits eight individual responses of radial electric dipoles numbered as shown in Fig. 3 (right). The last two columns consist of the sum of the responses and the 'ideal' CED response, respectively. All individual electric dipole responses as well as the response of the 'ideal' CED are calculated with an accuracy of at least three significant figures in the whole time range considered.

One can see that the sum of the individual responses coincides very well with the 'ideal' CED response up to approximately 8 ms. At later times, it becomes totally unstable despite of the fact that all individual responses are calculated with sufficiently high accuracy of at least three significant figures. The reason becomes perfectly clear, when the responses from opposite dipoles, that is 1 – 5, 2 – 6, 3 – 7 and 4 – 8, are considered. At late times, the absolute values of the responses in the pairs become very close to each other, whereas their polarities are obviously opposite at all times. Their algebraic sum thus cancels several significant figures and the result becomes randomly inaccurate. It is interesting to note that the above considered spectral algorithm becomes unstable in the same model at later times (Fig. 6). This means that even such a simple operation as a single summation could lead to greater errors than numerical calculation of oscillating double integrals.

Table 2 Transient responses of eight individual electric lines composing the 'real' CED (Fig. 3), their sum and the ideal CED responses for the same model as described in Fig. 6

Time (ms)	1	2	3	4	5	6	7	8	SUM	CED
1.00×10^{-01}	1.22×10^{-05}	5.64×10^{-06}	-6.41×10^{-09}	-2.10×10^{-06}	-2.63×10^{-06}	-2.10×10^{-06}	-6.41×10^{-09}	5.64×10^{-06}	1.66×10^{-05}	1.66×10^{-05}
1.20×10^{-01}	1.12×10^{-05}	5.44×10^{-06}	-6.41×10^{-09}	-2.09×10^{-06}	-2.62×10^{-06}	-2.09×10^{-06}	-6.41×10^{-09}	5.44×10^{-06}	1.53×10^{-05}	1.53×10^{-05}
1.45×10^{-01}	1.02×10^{-05}	5.15×10^{-06}	-6.41×10^{-09}	-2.07×10^{-06}	-2.60×10^{-06}	-2.07×10^{-06}	-6.41×10^{-09}	5.15×10^{-06}	1.37×10^{-05}	1.37×10^{-05}
1.75×10^{-01}	9.01×10^{-06}	4.78×10^{-06}	-6.41×10^{-09}	-2.04×10^{-06}	-2.57×10^{-06}	-2.04×10^{-06}	-6.41×10^{-09}	4.78×10^{-06}	1.19×10^{-05}	1.19×10^{-05}
2.10×10^{-01}	7.88×10^{-06}	4.35×10^{-06}	-6.41×10^{-09}	-1.98×10^{-06}	-2.51×10^{-06}	-1.98×10^{-06}	-6.41×10^{-09}	4.35×10^{-06}	1.01×10^{-05}	1.01×10^{-05}
2.54×10^{-01}	6.73×10^{-06}	3.86×10^{-06}	-6.41×10^{-09}	-1.89×10^{-06}	-2.41×10^{-06}	-1.89×10^{-06}	-6.41×10^{-09}	3.86×10^{-06}	8.24×10^{-06}	8.24×10^{-06}
3.05×10^{-01}	5.69×10^{-06}	3.36×10^{-06}	-6.41×10^{-09}	-1.78×10^{-06}	-2.28×10^{-06}	-1.78×10^{-06}	-6.41×10^{-09}	3.36×10^{-06}	6.57×10^{-06}	6.57×10^{-06}
3.68×10^{-01}	4.71×10^{-06}	2.86×10^{-06}	-6.41×10^{-09}	-1.63×10^{-06}	-2.10×10^{-06}	-1.63×10^{-06}	-6.41×10^{-09}	2.86×10^{-06}	5.05×10^{-06}	5.05×10^{-06}
4.43×10^{-01}	3.85×10^{-06}	2.40×10^{-06}	-6.41×10^{-09}	-1.47×10^{-06}	-1.90×10^{-06}	-1.47×10^{-06}	-6.41×10^{-09}	2.40×10^{-06}	3.79×10^{-06}	3.78×10^{-06}
5.34×10^{-01}	3.09×10^{-06}	1.97×10^{-06}	-6.41×10^{-09}	-1.29×10^{-06}	-1.68×10^{-06}	-1.29×10^{-06}	-6.41×10^{-09}	1.97×10^{-06}	2.75×10^{-06}	2.75×10^{-06}
6.43×10^{-01}	2.46×10^{-06}	1.59×10^{-06}	-6.41×10^{-09}	-1.10×10^{-06}	-1.46×10^{-06}	-1.10×10^{-06}	-6.41×10^{-09}	1.59×10^{-06}	1.95×10^{-06}	1.95×10^{-06}
7.74×10^{-01}	1.93×10^{-06}	1.26×10^{-06}	-6.41×10^{-09}	-9.26×10^{-07}	-1.23×10^{-06}	-9.26×10^{-07}	-6.41×10^{-09}	1.26×10^{-06}	1.35×10^{-06}	1.35×10^{-06}
9.33×10^{-01}	1.49×10^{-06}	9.86×10^{-07}	-6.40×10^{-09}	-7.60×10^{-07}	-1.02×10^{-06}	-7.60×10^{-07}	-6.40×10^{-09}	9.86×10^{-07}	9.06×10^{-07}	9.06×10^{-07}
1.12	1.14×10^{-06}	7.62×10^{-07}	-6.36×10^{-09}	-6.14×10^{-07}	-8.28×10^{-07}	-6.14×10^{-07}	-6.36×10^{-09}	7.62×10^{-07}	5.94×10^{-07}	5.94×10^{-07}
1.35	8.54×10^{-07}	5.76×10^{-07}	-6.23×10^{-09}	-4.83×10^{-07}	-6.55×10^{-07}	-4.83×10^{-07}	-6.23×10^{-09}	5.76×10^{-07}	3.71×10^{-07}	3.71×10^{-07}
1.63	6.29×10^{-07}	4.27×10^{-07}	-5.94×10^{-09}	-3.72×10^{-07}	-5.07×10^{-07}	-3.72×10^{-07}	-5.94×10^{-09}	4.27×10^{-07}	2.20×10^{-07}	2.19×10^{-07}
1.96	4.60×10^{-07}	3.14×10^{-07}	-5.45×10^{-09}	-2.83×10^{-07}	-3.87×10^{-07}	-2.83×10^{-07}	-5.45×10^{-09}	3.14×10^{-07}	1.24×10^{-07}	1.23×10^{-07}
2.36	3.32×10^{-07}	2.28×10^{-07}	-4.73×10^{-09}	-2.12×10^{-07}	-2.91×10^{-07}	-2.12×10^{-07}	-4.73×10^{-09}	2.28×10^{-07}	6.41×10^{-08}	6.42×10^{-08}
2.85	2.39×10^{-07}	1.64×10^{-07}	-3.85×10^{-09}	-1.57×10^{-07}	-2.16×10^{-07}	-1.57×10^{-07}	-3.85×10^{-09}	1.64×10^{-07}	3.03×10^{-08}	3.01×10^{-08}
3.43	1.74×10^{-07}	1.20×10^{-07}	-2.96×10^{-09}	-1.17×10^{-07}	-1.62×10^{-07}	-1.17×10^{-07}	-2.96×10^{-09}	1.20×10^{-07}	1.28×10^{-08}	1.29×10^{-08}
4.13	1.29×10^{-07}	8.95×10^{-08}	-2.14×10^{-09}	-8.83×10^{-08}	-1.22×10^{-07}	-8.83×10^{-08}	-2.14×10^{-09}	8.95×10^{-08}	4.82×10^{-09}	4.83×10^{-09}
4.98	9.72×10^{-08}	6.76×10^{-08}	-1.46×10^{-09}	-6.72×10^{-08}	-9.35×10^{-08}	-6.72×10^{-08}	-1.46×10^{-09}	6.76×10^{-08}	1.54×10^{-09}	1.55×10^{-09}
5.99	7.43×10^{-08}	5.19×10^{-08}	-9.59×10^{-10}	-5.18×10^{-08}	-7.22×10^{-08}	-5.18×10^{-08}	-9.59×10^{-10}	5.19×10^{-08}	4.11×10^{-10}	4.22×10^{-10}
7.22	5.70×10^{-08}	3.99×10^{-08}	-6.04×10^{-10}	-3.99×10^{-08}	-5.58×10^{-08}	-3.99×10^{-08}	-6.04×10^{-10}	3.99×10^{-08}	9.16×10^{-11}	9.17×10^{-11}
8.70	4.37×10^{-08}	3.06×10^{-08}	-3.70×10^{-10}	-3.06×10^{-08}	-4.30×10^{-08}	-3.06×10^{-08}	-3.70×10^{-10}	3.06×10^{-08}	9.40×10^{-12}	1.55×10^{-11}
1.05×10^{01}	3.32×10^{-08}	2.33×10^{-08}	-2.21×10^{-10}	-2.33×10^{-08}	-3.28×10^{-08}	-2.33×10^{-08}	-2.21×10^{-10}	2.33×10^{-08}	-2.00×10^{-12}	1.89×10^{-12}
1.26×10^{01}	2.52×10^{-08}	1.78×10^{-08}	-1.32×10^{-10}	-1.78×10^{-08}	-2.50×10^{-08}	-1.78×10^{-08}	-1.32×10^{-10}	1.78×10^{-08}	-3.00×10^{-12}	1.73×10^{-13}

5 CONCLUSIONS

The classical Tikhonov's method for solving one-dimensional boundary value problem for parabolic differential equation directly in time domain is generalized here for all major transmitter–receiver configurations generating both transverse electric (TE) and transverse magnetic (TM) fields in an arbitrary multi-layered model above an insulating or ideally conducting basement. In case of a finite conductivity/resistivity of the latter, the modelling is performed for a sufficiently large thickness of the last layer above the basement having the required finite conductivity/resistivity.

The solutions are represented in the form of real Fourier series rapidly converging at late times, thanks to the existence of an exponentially damped factor. This factor also allows easily obtaining analytical late-stage asymptotic solutions.

Comparison of rapidly damping responses calculated using different spectral algorithms for a model with an insulating basement shows that all of them fail at sufficiently late times, although the threshold time depends on the specific algorithm used. Contrary, the Tikhonov's method provides accurate results at arbitrarily late times in presence of an insulating or ideally conducting basement, but, if the latter has moderate resistivity, the accuracy of the results depends on the specific numerical algorithm used.

In case of conventional unimodal TE and mixed TE–TM fields, which decay at late times as a power of time, most of the modern spectral algorithms accurately calculate the response within a practically feasible time range. For these fields, the difference between spectral and Tikhonov's method is mainly of theoretical interest. The situation is entirely different for unimodal TM-fields, which decay much faster above both conductive and, particularly, resistive basements (in fact, exponentially, in case of an insulating and ideally conducting basements). In this case, even most accurate spectral algorithms become unstable at moderately late times, while the described direct time domain Tikhonov's method provides accurate results at any delay time. Although the latter observation is true for all direct time domain algorithms, such as numerical finite-difference (finite-element) and the hybrid integral-finite-difference ones, only the Tikhinov's solution provides convenient semi-analytical representation for the wide class of transmitter–receiver configurations and model types.

ACKNOWLEDGEMENTS

The authors would like to thank James Macnae and the anonymous reviewer for useful comments, which helped to clarify and improve the original manuscript.

ORCID

Mark Goldman https://orcid.org/0000-0003-4598-6195

REFERENCES

Anderson W.L. 1979. Computer program numerical integration of related Hankel transforms of orders 0 and 1 by adaptive digital filtering. *Geophysics* **44**, 1287–1305.

Barringer A.R. 1962. New approach to exploration; the INPUT airborne electric pulse prospecting system. *Mining Congress Journal* **48**, 49–52.

Barsukov P.O. and Fainberg E.B. 2017. Marine transient electromagnetic sounding of deep buried hydrocarbon reservoirs: principles, methodologies and limitations. *Geophysical Prospecting* **65**, 840–858.

Chave A. 1983. Numerical integration of related Hankel transforms by quadrature and continued fraction expansion. *Geophysics* **48**, 1671–1686.

Druskin V.L. and Knizhnerman L.A. 1988. Spectral differential-difference method for numeric solution of three-dimensional nonstationary problems of electric prospecting. *Izvestiya, Earth Physics* **24**, 641–648.

Epov M.I. and Eltsov I.N. 1992. *Forward and Inverse Problems of Inductive Geoelectrics in One Dimensional Media*. OGGiM SO RAN, Novosibirsk. (in Russian.)

Everett M.E. 2013. *Near-Surface Applied Geophysics*. Cambridge University Press.

Filon L. 1930. On a quadrature formula for trigonometric integrals. *Proceedings of the Royal Society of Edinburgh* **49**, 38–47.

Frischknect F.C. and Raab P.V. 1984. Time-domain electromagnetic soundings at the Nevada test site, Nevada. *Geophysics* **49**, 981–992.

Frolov P.P. 1965. On the asymptotic behavior of the transient field in a layered medium. *Izvestiya Akademii Nauk SSSR Seriya Fizika Zemli* **1**, 59. (in Russian.)

Goldman M. 1983. The integral-finite-difference method for calculating transient electromagnetic fields in a horizontally stratified medium. *Geophysical Prospecting* **31**, 664–686.

Goldman M. 1987. Forward modelling for frequency domain marine electromagnetic systems. *Geophysical Prospecting* **35**, 1042–1064.

Goldman M. and Fitterman D. 1987. Direct time-domain calculation of the transient response for a rectangular loop over a two-layered medium. *Geophysics* **52**, 997–1006.

Goldman M. and Mogilatov V. 1978. Transient field of a vertical electric dipole embedded in a horizontally layered half-space. In: *Theory and Applications of Electromagnetic Fields in Geophysical Exploration*, pp. 123–138. Izvestiya Akademii Nauk SSSR, Novosibirsk. (in Russian.)

Goldman M., Mogilatov V., Haroon A., Levi E. and Tezkan B. 2015. Signal detectability of marine electromagnetic methods in the exploration of resistive targets. *Geophysical Prospecting* **63**, 192–210.

Goldman M. and Stoyer C. 1983. Finite-difference calculations of the transient field of an axially symmetric earth for vertical magnetic dipole excitation. *Geophysics* **48**, 953–963.

Helwig S.L., Wahab El Kaffas A., Holten T., Frafjord Ø. and Eide K. 2013. Vertical dipole CSEM: technology advances and results from the Snøhvit field. *First Break* **31**, 63–68.

Holten T., Flekkøy E.G., Maløy K.J. and Singer B. 2009. Vertical source and receiver CSEM method in time-domain. 79th SEG Annual meeting, Houston, TX, Expanded Abstracts, 749–752.

Kamke E. 1977. Differentialgleichungen: Losungsmethoden und Losungen, I, Gewohnliche Differentialgleichungen, B. G. Teubner, Leipzig, 1977.

Kaufman A.A. and Keller G.V. 1983. *Frequency and Transient Sounding: Methods in Geochemistry and Geophysics*. Elsevier Science.

Kaufman A.A. and Morozova G.M. 1970. *Theoretical Basis for the Transient Sounding Method in the near Zone*. Nauka, Moscow. (in Russian.)

Knight J.H. and Raiche A.P. 1982. Transient electromagnetic calculations using the Gaver-Stehfest inverse Laplace transform method. *Geophysics* **47**, 47–50.

Korn G.M. and Korn T.M. 1968. *Mathematical Handbook for Scientists and Engineers*. McGraw-Hill.

Macnae J.C. 1984. Survey design for multicomponent electromagnetic systems. *Geophysics* **49**, 265–273.

McNeill J.D. 1980. Applications of transient EM techniques. Technical Note TN-7, Geonics Ltd, Ontario, Canada.

Mogilatov V. 1996. Excitation of a half-space by a radial current sheet source. *Pure and Applied Geophysics* **147**, 763–775.

Mogilatov V. 2014. *Pulse Geoelectrics*. Novosibirsk State University, Novosibirsk. (in Russian.)

Mogilatov V. and Balashov B. 1996. A new method of geoelectrical prospecting by vertical electric current soundings. *Journal of Applied Geophysics* **36**, 31–41.

Mogilatov V.S. 1993. On one method of a solution of the principal forward problem of geoelectrics. *Geol. i geof.* **3**, 108–117. (in Russian.)

Mogilatov V.S., Zlobinskiy A.V. and Balashov B.P. 2017. Transient electromagnetic surveys with unimodal transverse magnetic field: ideas and results. *Geophysical Prospecting* **65**, 1380–1397.

Nazarenko O. 1961. Electrical device for marine exploration. USSR patent 751834/26–10.

Newman G.A., Hohmann G.W. and Anderson W.L. 1986. Transient electromagnetic response of a three-dimensional body in a layered earth. *Geophysics* **51**, 1608–1627.

Obukhov G.G. 1970. Structural electrical prospecting using closely spaced source and receiver. *Prikladnaya Geofizika* **58**, 142–157. (in Russian.)

Pracser E. 1992. Fast computing of transient electromagnetic field on the surface of a layered halfspace. *Geofiz. kozl.* **37**, 159–176.

Sheinman S.M. 1947. On transient electromagnetic fields in the earth. *Prikladnaya Geofizika* **9**, 3–55. (in Russian.)

Sidorov V.A. and Tikshaev V.V. 1969. *Electrical Soundings with Transient Fields in the Near Zone*. NIGG, Nizhnevolzhskiy. (in Russian.)

Singer B.S. and Artamonova S. 2013. Vertical electric source in transient marine CSEM: effect of 3D inhomogeneities on the late time response. *Geophysics* **78**, E173–E188.

Singer B.S. and Green A. 2003. Transient field solution for a layer of finite thickness on a resistive basement. *Geophysics* **68**, 1232–1240.

Skugarevskaya O.A. 1959. Calculation of the late stage of a transient electric field in a three-layered medium. *Izvestiya Akademii Nauk SSSR, Seriya Geofizika* **1**, 59–72. (in Russian.)

Tabarovsky L. and Sokolov V. 1982. Software for calculating transient fields of dipole sources in horizontally layered medium (ALEX). In: *Electromagnetic Methods of Geophysical Research*, pp. 57–77. IGiG SOAN SSSR. (in Russian.)

Tabarovsky L.A. and Epov M.I. 1998. Discrete spectra in diffraction problems of transient field on the Sheinman's films. *Izvestiya Akademii Nauk SSSR Seriya Fizika Zemli* **9**, 46–54. (in Russian.)

Tikhonov A. 1950. On transient electric currents in an inhomogeneous layered medium. *Izvestiya Akademii Nauk SSSR Seriya geograf. i Geofizika* **14**, 199–222. (in Russian.)

Tikhonov A.N. 1946. On the transient electric current in a homogeneous conducting half-space. *Izvestiya Akademii Nauk SSSR Seriya Geograf. i Geofizika* **10**, 213–231. (in Russian.)

Tikhonov A.N. and Skugarevskaya O.A. 1950. On transient electrical current in heterogeneous medium. *Izvestiya Akademii Nauk SSSR Seriya Geograf. i Geofizika* **14**, 281–283. (in Russian.)

Um E.S., Alumbaugh D.L., Harris J.M. and Chen J. 2012. Numerical modeling analysis of short-offset electric-field measurements with a vertical electric dipole source in complex offshore environments. *Geophysics* **77**, E329–E341.

Vanyan L.L. 1962. New method of determining the electromagnetic field of a dipole grounded on the surface of a multilayered isotropic medium. *Geol. i Geofiz.* **12**. (in Russian.)

Wait J.R. 1971. On the theory of transient EM sounding over a stratified earth. *Canadian Journal of Physics* **50**, 1055–1061.

Wait J.R. 1997. Letter to editor. Comment on "Excitation of a half-space by a radial current sheet source" by V. Mogilatov. *Pure and Applied Geophysics* **150**, 155.

Wang T. and Hohmann G.W. 1993. A finite-difference, time-domain solution for three-dimensional electromagnetic modeling. *Geophysics* **58**, 797–809.